ARTICLE TEMPLATE

Attitude Estimation of Connected Drones based on Extended Kalman Filter under Real Outdoor Environments

Kento Fukuda[a] , Shin Kawai[a] and Hajime Nobuhara[a]

[a] Department of Intelligent Interaction Technologies, Graduate School of Systems and Information Engineering,University of Tsukuba, Ibaraki, Japan;

ARTICLE HISTORY
Compiled October 11, 2022

ABSTRACT
In this study, we design connected multiple drones through electromagnets, and it requires an attitude estimation that does not use magnetic sensors. In order to solve this problem, we propose an extended Kalman filter-based attitude estimation method based on the multiple global positioning system (GPS) to substitute the magnetic sensor. Additionally, we demonstrate that combining velocity vectors allows for highly accurate attitude estimation. We compare the estimation accuracy and stability of attitude estimation in simulation and real environments using two types of experiments. It is confirmed that the accuracy of yaw angle estimation of the proposed method is improved 36.1 % in simulation and 29.7 % in the real environments compared to conventional extended Kalman filter.

KEYWORDS
Connected Drone; RTK-GPS; Extended Kalman Filter; Multiple GPS; Attitude Estimation

1. Introduction

Recently, drone technology has been commonly used because of the drastic improvement of its performance and reduction in its manufacturing cost [1]. Therefore, drones have been used in various fields such as agriculture, forestry, surveying, inspection, disaster investigation, security, delivery, entertainment, and so on [2], and it has been attracting increasing attention every year. The use of drones in a single aircraft has been thoroughly studied and is now being expanded to include multiple drones.

Many studies have focused on cooperative flight as a flight mode for multiple drones. However, autonomous flight of multiple drones is difficult because of technical issues, such as the need for precise control to avoid collisions and the need for multiple communication channels for the drones to communicate with each other [3]. To solve this problem, we focus on a connected drone system. This is a system in which multiple drones can be physically connected and separated to function as different-size drones depending on the situation. This system allows the number of drones required for communication and collision avoidance to be changed as needed. Drones with connecting

CONTACT Kento Fukuda First Author Email: fukuda@cmu.iit.tsukuba.ac.jp ORCiD: 0000-0001-5222-4848
Shin Kawai Email: kawai@cmu.iit.tsukuba.ac.jp ORCiD: 0000-0003-3287-6093
Hajime Nobuhara Corresponding Author Email: nobuhara@cmu.iit.tsukuba.ac.jp ORCiD: 0000-0002-1818-6929

mechanisms are rarely seen, except for a few types of research and patents [4–7], that is, such systems have not been sufficiently considered or discussed.

The purpose of this study is that we focus on the application of multiple drones using this connection method, design the drones and present a suitable attitude estimation method for this drone. Fig. 1 shows an overview of the proposed drone.

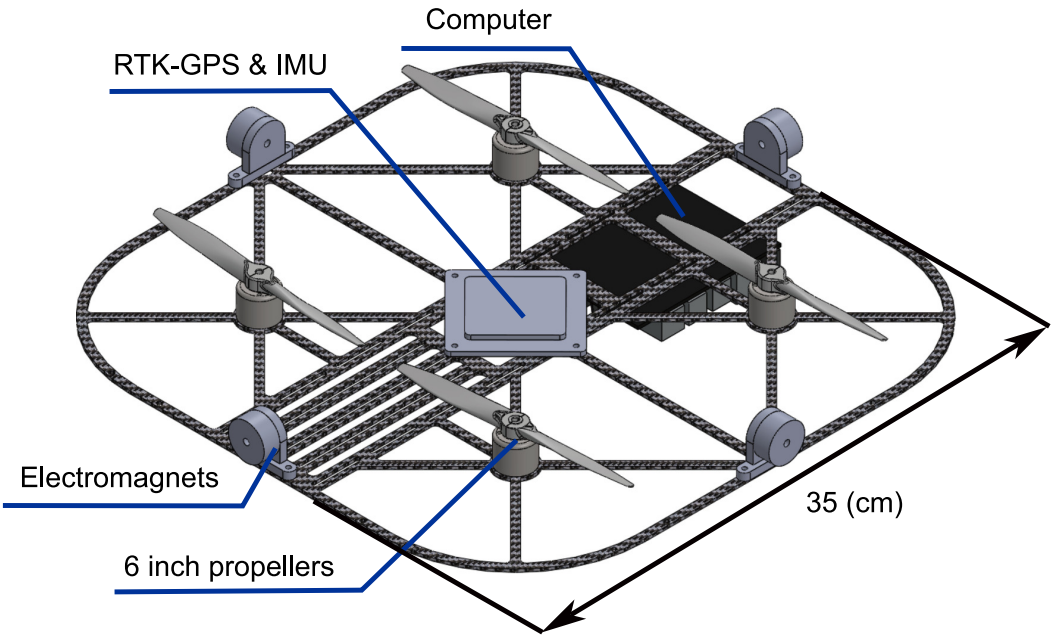

Figure 1. Drone Configuration

It is approximately 35 cm long on each side and has electromagnets on the four sides for the connecting mechanism. We use electromagnets for the connecting mechanism. This is because the magnetic force makes switching between connecting and separating each other drones easier and ensures a strong connecting force. This magnetic connecting mechanism makes flying like one large drone in various shapes possible. This mechanism minimises the size of a single drone but allows it to be operated flexibly depending on the task. In the centre, the drone has a global positioning system (GPS) and an inertial measurement unit (IMU). These sensors can measure its position, speed, acceleration and angular velocity. Furthermore, the system uses real-time kinematic GPS positioning. This positioning system allows the position to be measured with high accuracy.

In general, the measurement of a drone's self-attitude enables the control of its position and speed. Therefore, the self-attitude measurement of drones is necessary for stable and automatic control [8,9], and many researchers are working on attitude estimation methods. Presently, the Kalman filter (KF) is mainly used for drone attitude estimation [9]. KF is an algorithm that can be used to estimate the state of a system if the accurate dynamics model of the target is known and can be used to fusion various sensors [10]. This means that KF can combine the advantages and disadvantages of various sensors. Owing to its simplicity and low computational cost, KF is used in many fields other than attitude estimation [11]. However, KF has some disadvantages, such as it cannot be used in nonlinear models and is easily affected by modelling errors of the estimation target. To solve these disadvantages, KF has been developed in

various ways. For example, for targets that are difficult to adapt to nonlinear models, extended KF (EKF) is used to make a linear approximation around the estimated value [12], or unscented KF is used to approximate and estimate the state variables by applying the unscented transformation [13]. Besides, adaptive KF [14] and fuzzy KF [15] are used in cases where modelling errors are likely to occur, or the model changes dynamically. Sensor fusion methods have been studied using KF, including various sensors such as IMU [16–18], GPS [19], camera [20],millimetre wave radar [21], star tracker [22], barometer [23], and other sensors. Often, attitude estimation by KF used IMU, including a magnetic sensor.

Our proposed drone is connected using an electromagnet, disturbing the surrounding magnetic field. Due to disturbance, magnetic sensors, which are often used for attitude estimation, cannot be used. Therefore, we focused on a method [24,25] that substitutes the geomagnetic sensor with two GPS antennas, extended this to the case of three or more antennas, and applied it to our drone. Additionally, we add drone velocity to the observation equation of EKF for highly accurate attitude estimation.

Due to not using a magnetic sensor, our proposed drone can operate in a geomagnetic environment that was previously inaccessible to existing drones. For example, Park et al. studied magnetic disturbances around ultra-high-voltage wires [26]. Because our proposed drone does not rely on a magnetic sensor, it can be used for tasks such as inspecting ultra-high-voltage power lines.

The structure of this paper is as follows. In section 2, we introduce the previous studies on attitude estimation and the proposed method. We add the velocity term of the drone to the observation equation and try to make it more accurate than previous studies. In section 3, we verify the effectiveness of the proposed attitude estimation method through simulation experiments and outdoor experiments. In section 4 we draw conclusions. In our previous study [27], we used a simulation experiment to demonstrate the effectiveness of attitude estimation in a connected drone. In this study, the simulation situation was increased for further verification of effectiveness. Furthermore, the estimation experiment was conducted in the real environment, and the effectiveness of the real environment was also confirmed.

2. Methods

In this section, we introduce three conventional methods used for attitude estimation and describe the proposed method.

2.1. Conventional methods

In this section, we introduce the Q-Method, the Madgwick filter (MF) and the KF, which are used for attitude estimation.

2.1.1. Estimation by the Q-Method

Inoue et al. proposed a method for estimating the attitude of drones using the Q-Method [28]. The Q-Method is a method mainly used for satellite attitude estimation, which uses star tracker and sun sensors attached to the satellite to estimate its self attitude [29]. Specifically, the attitude is estimated by computing an attitude that minimises an attitude estimation error function called the Wahba evaluation formula [30]. Inoue et al. applied this method to the attitude estimation of a drone with

six RTK-GPS antennas. The advantage of this method is that it is a static estimation method and is not affected by large past noises. However, the disadvantage is that the estimation accuracy varies greatly depending on the number of GPS antennas, especially when there are fewer than two antennas, the estimation is almost impossible. In the section 3.1 we verify that this method is suitable for our proposed drone attitude estimation.

2.1.2. Estimation by the Madgwick filter

Madgwick has proposed a method of attitude estimation called the MF, which uses only an IMU or an IMU and a magnetic sensor [31]. One of the features of this method is that it reduces the computational load while achieving the same accuracy as the KF method of estimation. The method determines the attitude by calculating a weighted average of two attitude estimates, one using the gyro sensor and the other using only the acceleration sensor or both the acceleration and magnetic sensor. This method gives relatively good accuracy but has the disadvantage that the accuracy decreases when the object is moving because it uses the direction of gravity. It has been suggested that this drawback can be solved using a magnetic sensor [31]. However, this solution cannot be used because magnetic sensors are unavailable for this drone. In section 3.1, we will verify how accurately we can estimate the attitude without using a magnetic sensor.

2.1.3. Estimation by the EKF

Farhad et al. proposed an attitude estimation method suitable for rovers with two GPS antennas and an IMU [24]. In this proposal, they have focused on the adaptive EKF. The adaptive EKF is an algorithm proposed to deal with systems where the internal state is changing, allowing the simultaneous estimation of the state and noise variance matrices [32]. The Farhad et al. method uses an adaptive EKF to estimate state variables such as attitude, position, velocity and gyro bias noise. By using the adaptive EKF, they could reduce the effects of accumulated noise, which is a disadvantage of IMU and increases the estimation frequency, which is a disadvantage of GPS. Furthermore, it is flexible enough to adapt to changes in the environment by estimating the GPS noise variance matrices as it changes with movement and time. We focus on this method and propose its application to our connected drone. We have calculated the case of multiple IMUs and made them available for use in connected drones. Furthermore, we have improved the accuracy by adding the drone's velocity obtained from GPS to the observation vector. This velocity data is provided using the Doppler effect of the transmitted waves from the GPS. Section 3.1 examines the effectiveness of this method.

2.2. Proposed method

Figure 1 shows the configuration of a single drone. The drone has an IMU and a GPS antenna in the centre and electromagnets for the coupling mechanism on its four sides. In this study, we consider the attitude estimation with two laterally connected drones as shown in Fig. 2.
We describe the mathematical symbols we use in section 2.2 below. The estimated value of the signal f is expressed by $\hat{f}$, and the difference between the true value f of the signal and the estimated value $\hat{f}$ is expressed by δf, where this difference is

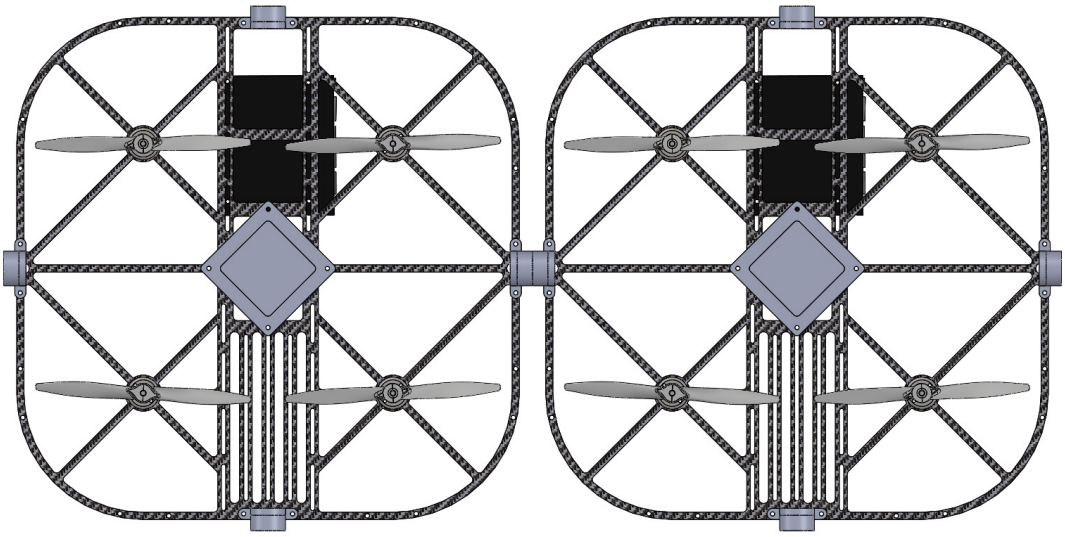

Figure 2. After the Connection

called the residual. That is, $x - \hat{x} = \delta x$ is held for a given estimated signal x. The bold symbol $\boldsymbol{f}$ represents a vector.

2.2.1. Coordinate systems

We introduced two coordinate systems, such as those shown in Fig. 3 for attitude estimation.
The first is the World coordinate system, which is a system in which the origin is the position of the reference antenna, the east direction is the X_W axis, the north direction is the Y_W axis, and the reverse direction of gravity is the Z_W axis. The second system is the Body coordinate system, which uses the X_B axis to represent the forward direction, Y_B axis to represent the right and left directions, Z_B axis to represent the up and down directions, and the origin as the centre of the two GPS antennas. This coordinate system is attached to the drone, where the position and attitude change with its motion. The estimation is the attitude of the Body coordinate system in the World coordinate system, the GPS value is the value of the World coordinate system, and the IMU value is the value of the Body coordinate system. Let the origin R of the Body coordinate system viewed from the World coordinate system be the point of estimation by the EKF. The positions of the respective antennas in the World coordinate system are P_1 and P_2. Furthermore, let $\boldsymbol{r}$ be the vector from the origin of the world coordinate system to point R and $\boldsymbol{p}_i$ be the vector to point P_i.

2.2.2. Quaternion deployment

The quaternion $\boldsymbol{q} \in \mathbb{R}^4$ expresses the attitude of the Body coordinate system from the World coordinate system. The advantage of using the quaternion is that no singularity point occurs when using Euler angles [33]. Generally, attitude control is impossible in singularity points. The quaternion expresses the attitude by using a four-dimensional

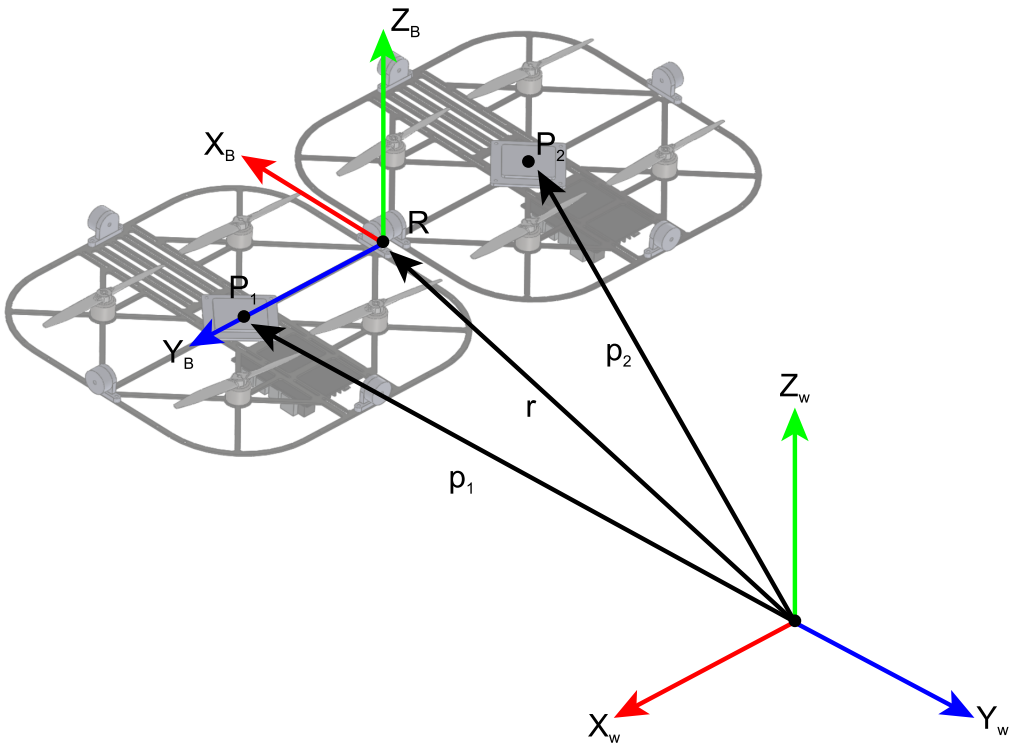

Figure 3. Body Coordinate and World Coordinate

vector $\boldsymbol{q} = [\boldsymbol{q}_v^T \ q_o]^T$. The quaternion,

$$\boldsymbol{q} = \begin{bmatrix} \boldsymbol{q}_v \\ q_o \end{bmatrix} \triangleq \begin{bmatrix} \lambda_x \sin\frac{\theta}{2} \\ \lambda_y \sin\frac{\theta}{2} \\ \lambda_z \sin\frac{\theta}{2} \\ \cos\frac{\theta}{2} \end{bmatrix}, \tag{1}$$

means θ rotation about the direction vector $\boldsymbol{q}_v \in \mathbb{R}^3$, where λ_x, λ_y, and λ_z are the unit direction vector, which is the axis of rotation of the quaternion. All the quaternions treated in this study are in the unit of size $\|\boldsymbol{q}\| = 1$, where $\|\cdot\|$ represents the Euclidean norm of the vector. The rotation matrix is given as,

$$A(\boldsymbol{q}) = (2q_o^2 - 1)I_3 + 2q_o[\boldsymbol{q}_v\times] + 2\boldsymbol{q}_v\boldsymbol{q}_v^T. \tag{2}$$

Here, I_3 is a unit matrix of 3×3, and $[\times]$ is a representation matrix of the vector product satisfying $\boldsymbol{a} \times \boldsymbol{b} = [\boldsymbol{a}\times]\boldsymbol{b}$ in the vector product. For example, the expression matrix of the vector product of $\boldsymbol{q}_v$ is equal to

$$[\boldsymbol{q}_v\times] = \begin{bmatrix} 0 & -q_z & q_y \\ q_z & 0 & -q_x \\ -q_y & q_x & 0 \end{bmatrix}. \tag{3}$$

Furthermore, the product of the quaternions is defined as

$$\boldsymbol{q}\otimes \triangleq q_o I_4 + \Omega(\boldsymbol{q}_v), \tag{4}$$

$$\Omega(\boldsymbol{q}_v) = \begin{bmatrix} -[\boldsymbol{q}_v\times] & \boldsymbol{q}_v \\ -\boldsymbol{q}_v^T & 0 \end{bmatrix}. \tag{5}$$

At this time,

$$A(\boldsymbol{q}_1 \otimes \boldsymbol{q}_2) = A(\boldsymbol{q}_2)A(\boldsymbol{q}_1), \tag{6}$$

is given. In a quaternion, the relationship between the true value $\boldsymbol{q}$, the estimated value $\hat{\boldsymbol{q}}$, and the residual $\delta\boldsymbol{q}$ is

$$\boldsymbol{q} = \delta\boldsymbol{q} \otimes \hat{\boldsymbol{q}}. \tag{7}$$

If the difference between $\boldsymbol{q}$ and $\hat{\boldsymbol{q}}$ is significantly small, the rotation angle $\delta\theta$ of the residual $\delta\boldsymbol{q}$ is so small that Eq. (1) yields $\|\delta\boldsymbol{q}_v\| \ll 1, \delta q_o \approx 1$. Therefore, if we truncate the small quantities of the order two or more from Eq. (2), an approximation like

$$A(\delta\boldsymbol{q}) \approx I_3 + 2[\delta\boldsymbol{q}_v\times], \tag{8}$$

can be held for the rotation matrix of the residuals.

If the angular velocity vector of the object is $\boldsymbol{\omega} \in \mathbb{R}^3$, the time derivative of the quaternion $\dot{\boldsymbol{q}}$ can be calculated as

$$\dot{\boldsymbol{q}} = \frac{1}{2}\Omega(\boldsymbol{\omega})\boldsymbol{q}. \tag{9}$$

When the angular velocity is measured using a gyro sensor, the bias noise $\boldsymbol{b} \in \mathbb{R}^3$ and random noise $\boldsymbol{w}_g \in \mathbb{R}^3$ are added to the measured value $\boldsymbol{u}_g \in \mathbb{R}^3$. Where $\boldsymbol{w}_g$ is the random walk noise according to $E[\boldsymbol{w}_g\boldsymbol{w}_g^T] = \sigma_g^2 I_3$. Additionally, according to [34], the gyro-bias is assumed to be $\dot{\boldsymbol{b}} = \boldsymbol{w}_b$, where $\boldsymbol{w}_b$ is a random walk noise that follows $E[\boldsymbol{w}_g\boldsymbol{w}_g^T] = \sigma_b^2 I_3$. The angular velocity vector $\boldsymbol{\omega}$ of the drone is calculated using the measured value $\boldsymbol{u}_g$, and the noise $\boldsymbol{b}, \boldsymbol{w}_g$ is calculated as

$$\boldsymbol{\omega} = \boldsymbol{u}_g - \boldsymbol{b} - \boldsymbol{w}_g. \tag{10}$$

The time derivative of the residual quaternion $\delta\boldsymbol{q}$ is satisfied from [34] as

$$\dot{\delta\boldsymbol{q}_v} = -[\hat{\boldsymbol{\omega}}\times]\delta\boldsymbol{q}_v - \frac{1}{2}\delta\boldsymbol{b} - \frac{1}{2}\boldsymbol{w}_g, \tag{11}$$

$$\dot{\delta q_o} = 0. \tag{12}$$

In the EKF, we estimated the vector part $\boldsymbol{q}_v$ of the attitude quaternion of the Body coordinate system as seen from the World coordinate system, the position vector $\boldsymbol{r} \in \mathbb{R}^3$, and the velocity vector $\dot{\boldsymbol{r}} \in \mathbb{R}^3$, of the Body coordinate system as shown in the World coordinate system, and the bias $\boldsymbol{b}$ that is used in the gyro sensor. Let $\boldsymbol{x} = [\boldsymbol{q}_v^T\ \boldsymbol{r}^T\ \dot{\boldsymbol{r}}^T\ \boldsymbol{b}^T]^T$ be the state estimation vector that combines them.

2.2.3. IMU integration

The IMU position in the conventional method [24] is at the centre of the body, whereas in this study, the IMU position is the antenna position. This study examines whether a measuring device installed at the antenna position can estimate the value of the drone's centre. In this study, we considered an n number of antennas. The vector to the antenna installation point in the World coordinate system shall be $\boldsymbol{p}_i \in \mathbb{R}^3, i = \{1, 2, \ldots, n\}$, and the acceleration and angular velocity at the point $\boldsymbol{p}_i$ shall be $\boldsymbol{a}_i, \boldsymbol{\omega}_i \in \mathbb{R}^3$. Let $\boldsymbol{a}, \boldsymbol{\omega} \in \mathbb{R}^3$ represent the acceleration and angular velocity, respectively at the centre point R after the connection, assuming that the connected drone rotates around the point R as a rotation vector $\boldsymbol{\omega}$. Furthermore, let $\boldsymbol{e}_i \in \mathbb{R}^3$ be the vector from the point R in the Body coordinate system to the position $\boldsymbol{p}_i$ of each antenna. Additionally, the relationship between $\boldsymbol{a}, \boldsymbol{\omega}$, $\boldsymbol{a}_i$ and $\boldsymbol{\omega}_i$, will be considered. Because the value of the angular velocity of a rigid body does not depend on its position, $\boldsymbol{\omega}$ can be calculated using the average value of the i-th $\boldsymbol{\omega}_i$ as

$$\boldsymbol{\omega} = \frac{\sum_{i=1}^{n} \boldsymbol{\omega}_i}{n}. \tag{13}$$

Here, the number of drones connected is $n \in \mathbb{R}$. If the weight of a single drone is $m \in \mathbb{R}$, the total weight after the connection is nm, where the external force applied to the i-th drone is $\boldsymbol{F}_i \in \mathbb{R}^3$ in a rotational coordinate system defined as Fig. 4. The equation of motion is given by

$$m\boldsymbol{a}_i = \boldsymbol{F} - 2m[\boldsymbol{\omega}\times]\dot{\boldsymbol{e}}_i - m[\boldsymbol{\omega}\times]([\boldsymbol{\omega}\times]\boldsymbol{e}_i). \tag{14}$$

Therefore, the sum of the equations of motion at the point $\boldsymbol{p}_i$ in the Body coordinate system can be expressed as

$$m\sum_{i=1}^{n} \boldsymbol{a}_i = \sum_{i=1}^{n} \boldsymbol{F}_i - 2m[\boldsymbol{\omega}\times]\sum_{i=1}^{n} \dot{\boldsymbol{e}}_i - m[\boldsymbol{\omega}\times]^2 \sum_{i=1}^{n} \boldsymbol{e}_i. \tag{15}$$

Here, if $\sum_{i=1}^{n} \boldsymbol{e}_i = \boldsymbol{0}$, Eq. (15), can be transformed into

$$\sum_{i=1}^{n} \boldsymbol{a}_i = \frac{\sum_{i=1}^{n} \boldsymbol{F}_i}{m}. \tag{16}$$

From the overall equation of motion, the acceleration $\boldsymbol{a}$ can be represented as

$$\boldsymbol{a} = \frac{\sum_{i=1}^{n} \boldsymbol{F}_i}{nm}. \tag{17}$$

Therefore, the acceleration $\boldsymbol{a}$ can be obtained from Eq. (16) and Eq. (17) using an average value as

$$\boldsymbol{a} = \frac{\sum_{i=1}^{n} \boldsymbol{a}_i}{n}. \tag{18}$$

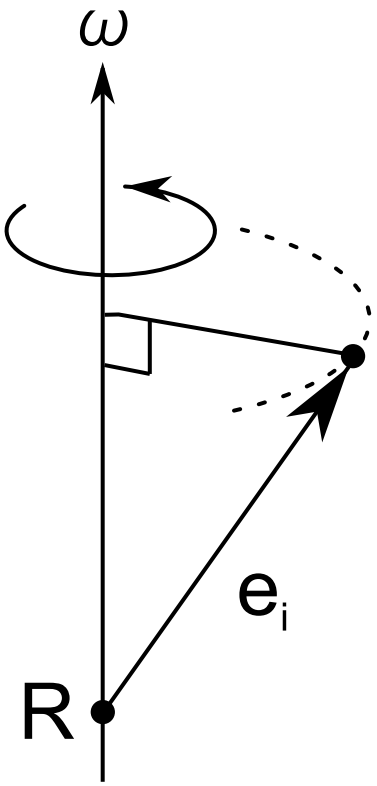

Figure 4. Rotational Coordinate System

2.2.4. Derivation of observation equations and Jacobian Matrices

Let $\dot{\boldsymbol{p}}_i$ be the velocity vectors obtained from the i-th GPS. When using a state vector to express the observation information, $\boldsymbol{p}_i, \dot{\boldsymbol{p}}_i$, can be obtained as shown below when there is no noise.

$$\boldsymbol{p}_i = \boldsymbol{r} + A(\boldsymbol{q})\boldsymbol{e}_i, \tag{19}$$

$$\dot{\boldsymbol{p}}_i = \dot{\boldsymbol{r}} + \dot{A(\boldsymbol{q})}\boldsymbol{e}_i. \tag{20}$$

However, this expression can be written as

$$\boldsymbol{z} = h(\boldsymbol{x}) + \boldsymbol{v}, \tag{21}$$

$$\boldsymbol{z} = \begin{bmatrix} \boldsymbol{p}_1 \\ \vdots \\ \boldsymbol{p}_n \\ \dot{\boldsymbol{p}}_1 \\ \vdots \\ \dot{\boldsymbol{p}}_n \end{bmatrix}, h(\boldsymbol{x}) = \begin{bmatrix} \boldsymbol{r} + A(\boldsymbol{q})\boldsymbol{e}_1 \\ \vdots \\ \boldsymbol{r} + A(\boldsymbol{q})\boldsymbol{e}_n \\ \dot{\boldsymbol{r}} + \dot{A(\boldsymbol{q})}\boldsymbol{e}_1 \\ \vdots \\ \dot{\boldsymbol{r}} + \dot{A(\boldsymbol{q})}\boldsymbol{e}_n \end{bmatrix}, \tag{22}$$

using the observation vector $\boldsymbol{z} \in \mathbb{R}^{3\times 2n}$, the observation equation $h(\boldsymbol{x}) \in \mathbb{R}^{3\times 2n}$, and the GPS observation noise $\boldsymbol{v} \in \mathbb{R}^{3\times 2n}$. To apply the nonlinear function $h(\boldsymbol{x})$ to the EKF, the Jacobian matrix must be calculated. This, the Jacobian matrix for $\boldsymbol{p}_i$ can be represented according to [24],

$$\left.\frac{\partial \boldsymbol{p}_i}{\partial \boldsymbol{x}}\right|_{\boldsymbol{x}=\hat{\boldsymbol{x}}} = \begin{bmatrix} -2\hat{A}[\boldsymbol{e}_i\times] & I_3 & 0_3 & 0_3 \end{bmatrix}, \tag{23}$$

where 0_3 represents a zero matrix of 3×3, and $\hat{A}$ represents $A(\hat{q})$. The Jacobian matrix for $\dot{\boldsymbol{p}}_i$ is then computed. The properties of the Jacobian matrix are

$$\delta\dot{\hat{\boldsymbol{p}}}_i = \left.\frac{\partial \dot{\boldsymbol{p}}_i}{\partial \boldsymbol{x}}\right|_{\boldsymbol{x}=\hat{\boldsymbol{x}}} \delta\boldsymbol{x}. \tag{24}$$

From the calculations shown in Appendix A, Eq. (24) becomes

$$\delta\dot{\hat{\boldsymbol{p}}}_i \approx \begin{bmatrix} 2(\hat{A}[\boldsymbol{e}_i\times][\hat{\boldsymbol{\omega}}\times] - \dot{\hat{A}}[\boldsymbol{e}_i\times]) & 0_3 & I_3 & \hat{A}[\boldsymbol{e}_i\times] \end{bmatrix} \delta\boldsymbol{x}. \tag{25}$$

Thus, the Jacobian matrix H for the observation equation $h(\boldsymbol{x})$ is calculated.

$$H = \left.\frac{\partial h(\boldsymbol{x})}{\partial \boldsymbol{x}}\right|_{\boldsymbol{x}=\hat{\boldsymbol{x}}} \tag{26}$$

$$= \begin{bmatrix} -2\hat{A}[\boldsymbol{e}_1\times] & I_3 & 0_3 & 0_3 \\ \vdots & \vdots & \vdots & \vdots \\ -2\hat{A}[\boldsymbol{e}_n\times] & I_3 & 0_3 & 0_3 \\ 2(\hat{A}[\boldsymbol{e}_1\times][\hat{\boldsymbol{\omega}}\times] - \dot{\hat{A}}[\boldsymbol{e}_1\times]) & 0_3 & I_3 & \hat{A}[\boldsymbol{e}_1\times] \\ \vdots & \vdots & \vdots & \vdots \\ 2(\hat{A}[\boldsymbol{e}_n\times][\hat{\boldsymbol{\omega}}\times] - \dot{\hat{A}}[\boldsymbol{e}_n\times]) & 0_3 & I_3 & \hat{A}[\boldsymbol{e}_n\times] \end{bmatrix}. \tag{27}$$

We can add observations of the velocity using Eq. (27) and Eq. (22), if we use them instead of the Jacobian matrix H and the observation equation $h(\boldsymbol{x})$ shown by the conventional method [24].
According to [24], the dynamics of this system is

$$\dot{\boldsymbol{x}} = f(\boldsymbol{x}, \boldsymbol{u}, \boldsymbol{w}) = \begin{bmatrix} \frac{1}{2}[I_3\ 0_{3\times1}][\Omega(\boldsymbol{u}_g + \boldsymbol{b} + \boldsymbol{w}_g)\boldsymbol{q}] \\ \dot{\boldsymbol{r}} \\ A(\boldsymbol{q})(\boldsymbol{u}_a + \boldsymbol{w}_a) - \boldsymbol{g} \\ \boldsymbol{w}_b \end{bmatrix}. \tag{28}$$

Where $\boldsymbol{u}_a$ is the value output from the acceleration sensor. Furthermore, $\boldsymbol{w}_a$ is the random walk noise added to the acceleration sensor, $E[\boldsymbol{w}_a\boldsymbol{w}_a^T] = \sigma_a^2 I_3$ is assumed. Moreover, $\boldsymbol{u}$ is $[\boldsymbol{u}_g^T\ \boldsymbol{u}_a^T]$, $\boldsymbol{w}$ is $[\boldsymbol{w}_g^T\ \boldsymbol{w}_b^T\ \boldsymbol{w}_a^T]^T$. The Jacobi matrix in equation Eq. (28) is

$$F = \left.\frac{\partial f}{\partial \boldsymbol{x}}\right|_{\boldsymbol{x}=\hat{\boldsymbol{x}},\boldsymbol{u}=\hat{\boldsymbol{u}}} = \begin{bmatrix} -[\hat{\boldsymbol{\omega}}\times] & 0_3 & 0_3 & \frac{1}{2}I_3 \\ 0_3 & 0_3 & I_3 & 0_3 \\ -2\hat{A}[\hat{\boldsymbol{a}}\times] & 0_3 & 0_3 & 0_3 \\ 0_3 & 0_3 & 0_3 & 0_3 \end{bmatrix}. \tag{29}$$

3. Experiments

In this section, we demonstrate the effectiveness of the proposed method through estimation simulations and outdoor experiments under various situations. We assume that the number of connections is two because attitude estimation is most difficult due to the number of sensors. We experiment with a situation where drones are connected side by side, as shown in Fig. 2. We use the Euler angle for accuracy evaluation because it is more intuitive than quaternions. The Euler angle consists of three rotation angles, roll, pitch and yaw angles, which represent the rotation around x-, y- and z-axes, respectively. In this study, the World coordinate system rotates with respect to the Body coordinate system in the order of yaw, pitch and roll.

3.1. Simulation Experiment

In this section, the accuracy of the attitude estimation is verified by simulation. In section 3.1.1, we experimented with the situation in which moving and rotating were

repeated. In section 3.1.2, we investigated the situation in which stopping and rotating were repeated. Four methods were used for comparison: the Q-Method, the MF, the conventional EKF using position information from GPS, and the proposed EKF using position and velocity information from GPS. Because the EKF is a stochastic method, the simulation experiments in each section are repeated 100 times under the same conditions, and the mean absolute error (MAE) and root mean square error (RMSE) is calculated from the results. The standard deviation values for the white noise added to each sensor are $\sigma_{\mathrm{gps}} = 2.0 \times 10^{-2}$ (m), $\sigma_{\mathrm{a}} = 2.5 \times 10^{-2}$ (m/s^2) and $\sigma_{\mathrm{g}} = 5.0 \times 10^{-2}$ (°/s).

3.1.1. Experimental results (moving and rotating)

In this section, we conducted an estimation experiment assuming a situation where the drone repeatedly moves in a straight line and rotates. Specifically, we assumed the estimation experiment is based on the assumption that the drone alternates between rotational and linear motion along the path shown in Fig. 5.

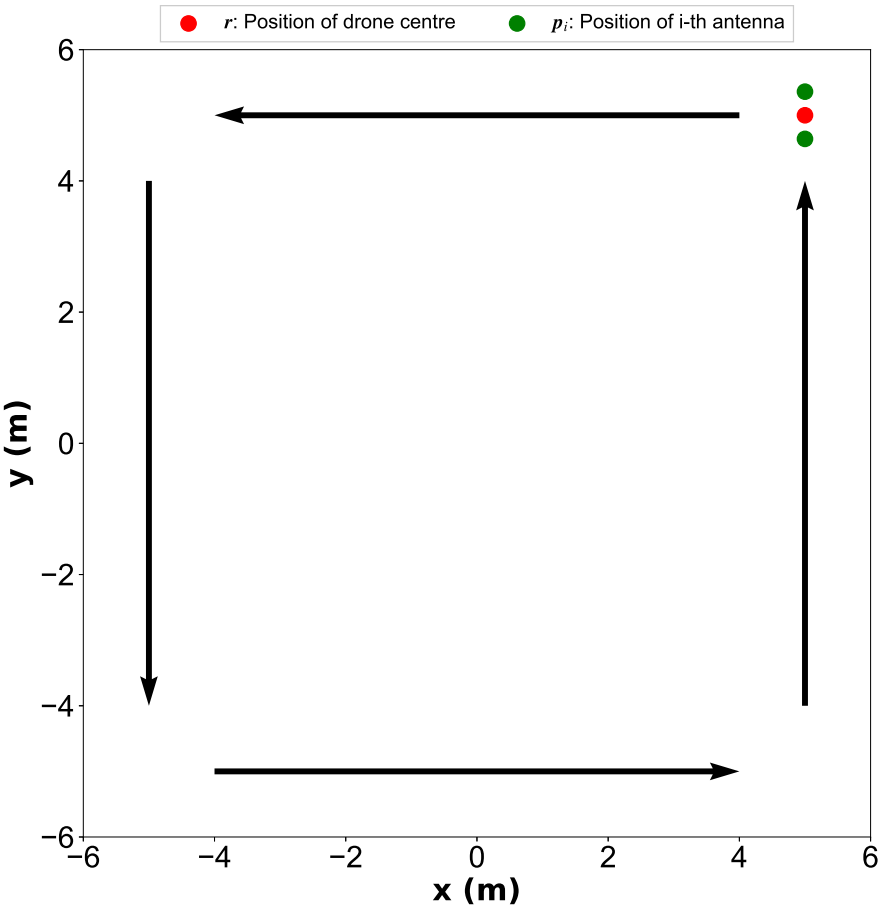

Figure 5. Drone Route in a Simulation

The red point in the Fig. 5 represents the drone's centre position $\boldsymbol{r}$ estimated by the EKF, and the green point represents the antenna position $\boldsymbol{p}_i$. Figs 6 and 7 show the experiment result for each methods.
Figure 8 shows the absolute error of Fig. 7 compared to the true value.
Table 1 summarises the MAE and RMSE of the experimental results.

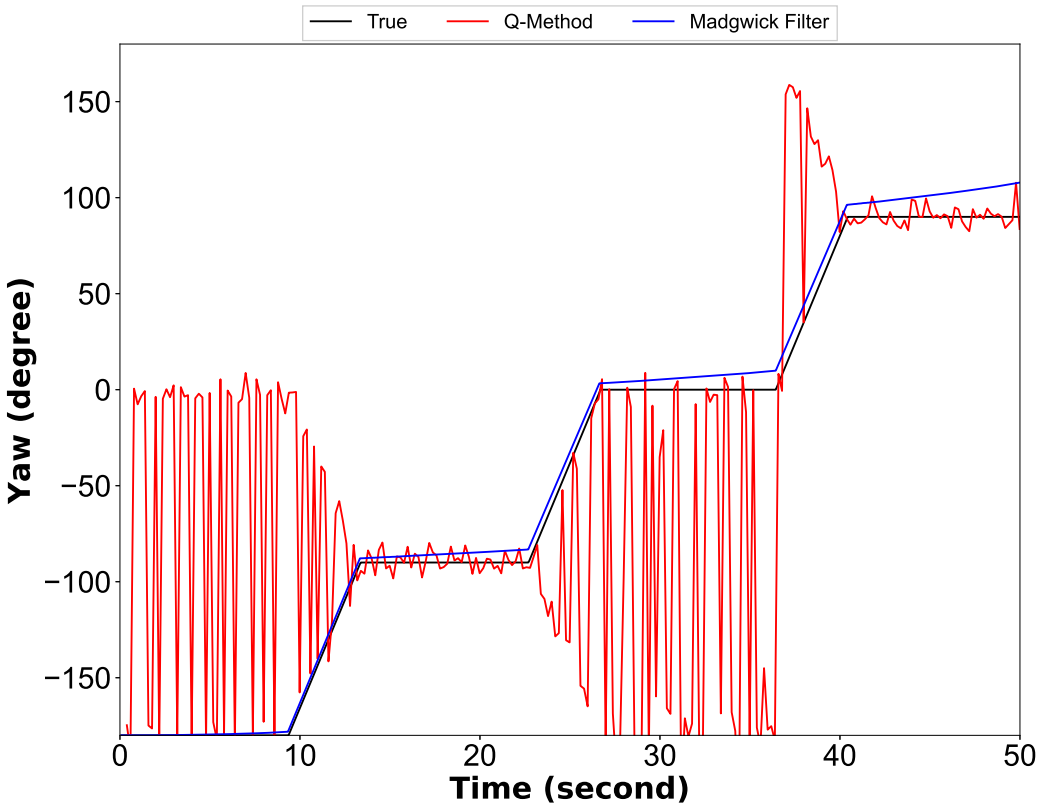

Figure 6. Attitude Estimation Results of Q-Method and Madgwick Filter (Simulation Experiment of Moving and Rotating)

Table 1. Comparison of Move And Rotate Estimation Results

	Roll Angle (°)		Pitch Angle (°)		Yaw Angle (°)	
	MAE	RMSE	MAE	RMSE	MAE	RMSE
Q-Method[29]	116	142	13.0	25.0	36.1	76.0
MF[31]	0.766	1.38	1.39	1.75	5.35	8.28
Conventional EKF[24]	1.29	1.29	0.954	1.20	1.04	1.26
Proposed EKF	**0.386**	**0.480**	**0.490**	**0.597**	**0.975**	**1.20**

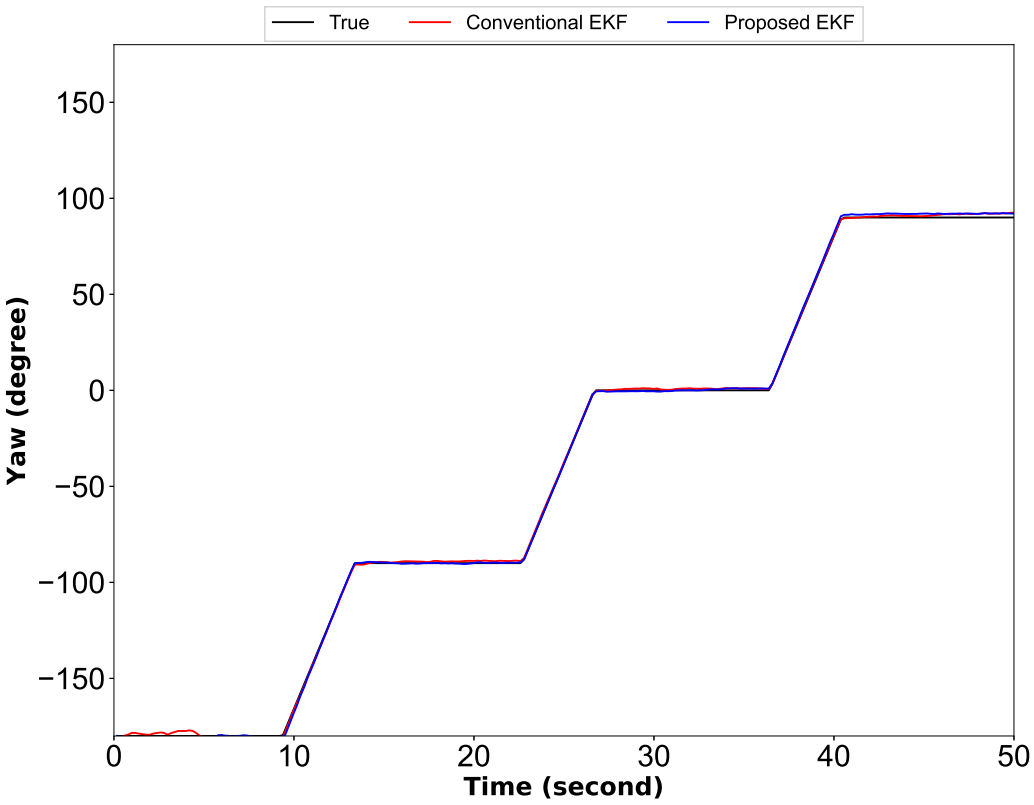

Figure 7. Attitude Estimation Results of Conventional EKF and Proposed EKF (Simulation Experiment of Moving and Rotating)

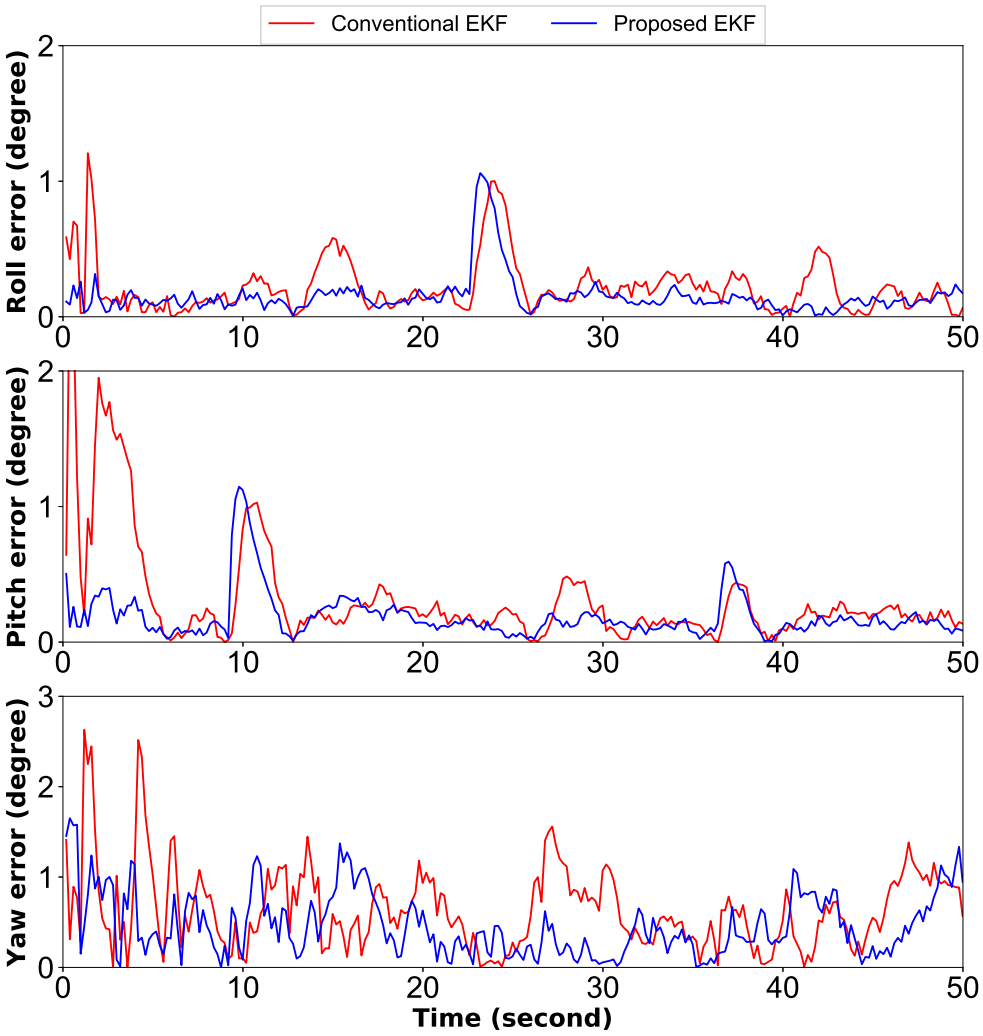

Figure 8. Absolute Error of Attitude Estimation Results of Conventional EKF and Proposed EKF(Simulation Experiment of Moving and Rotating)

Compared with the conventional method, the proposed method improved the MAE by 70.0 % for roll angle, 48.7 % for pitch angle and 5.96 % for yaw angle. Furthermore, for RMSE, the proposed method improved the roll angle by 70.4 %, pitch angle by 50.3 % and yaw angle by 4.77 %. Thus, these results show the effectiveness of our proposal.

3.1.2. Experimental results (stopping and rotating)

In this section, we conducted an estimation experiment assuming a situation where the drone repeatedly stops and rotates to verify the responsiveness in the stopped state. Specifically, we hypothetically assumed that the drone rotates at a speed of 1 degree per second for 30 s and then stops for 1 min, repeat the sequence of operations 12 times. Fig. 9 show the experiment result for each methods.

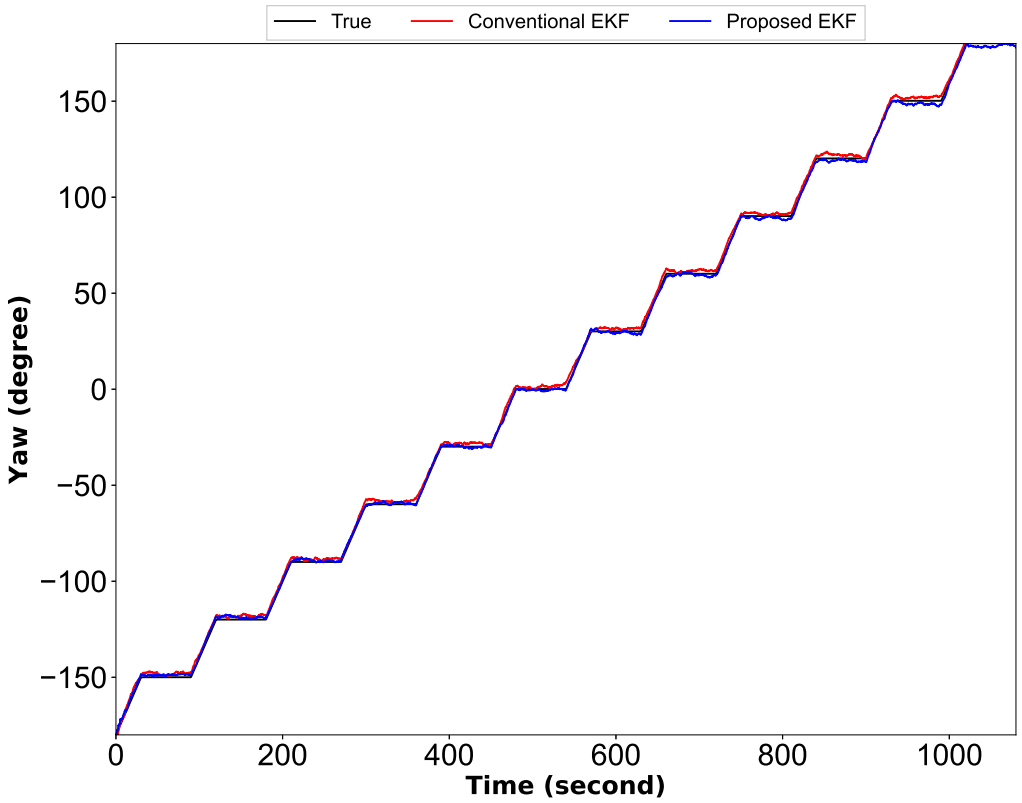

Figure 9. Attitude Estimation Results of Conventional EKF and Proposed EKF (Simulation Experiment of Stopping and Rotating)

Figure 10 shows the absolute error of Fig. 9 compared to the true value.
Table 2 summarises the MAE and RMSE of the experimental results.
The results show that the proposed method is the most accurate for MAE and RMSE of rotation on each axis. Specifically, compared with the conventional EKF, the proposed EKF improves the roll angle by approximately 73 %, the pitch angle by approximately 58 %, and the yaw angle by approximately 30 % for MAE and RMSE.

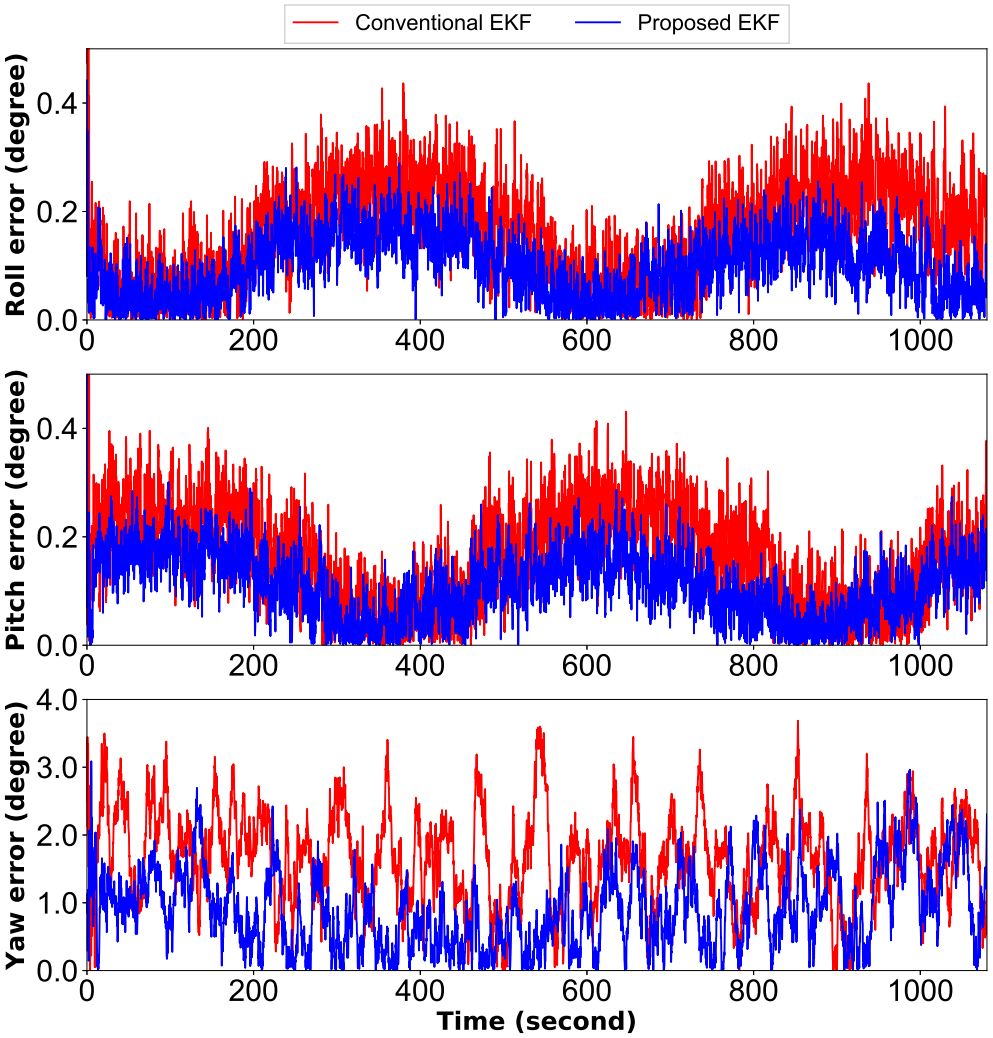

Figure 10. Absolute Error of Attitude Estimation Results of Conventional EKF and Proposed EKF(Simulation Experiment of Stopping and Rotating)

Table 2. Comparison of Stop And Rotate Estimation Results

	Roll Angle (°)		Pitch Angle (°)		Yaw Angle (°)	
	MAE	RMSE	MAE	RMSE	MAE	RMSE
Q-Method[29]	126	148	8.15	16.7	65.4	88.1
MF[31]	0.698	0.826	0.705	0.836	147	179
Conventional EKF[24]	1.44	1.77	0.848	1.03	1.86	2.22
Proposed EKF	**0.385**	**0.479**	**0.349**	**0.434**	**1.43**	**1.80**

3.1.3. Discussion of simulation experiments

Estimation results using the Q-Method (red line in Fig. 6) shows that the results of attitude estimation is unstable. This error is because Q-Method can not estimate attitude when the number of antennas is two. Q-Method estimation requires at least three antennas to obtain a unique attitude. In this study, we consider the number of connections to be at least two, so it is considered that the proposed system has difficulty in estimating the attitude using Q-Method.

The blue line in Fig. 6 shows that the estimation result is getting worse with time. This error is owing to a poor estimation of the bias noise added to the gyro sensor. As the effect of the bias noise increases with time, the estimate deteriorates with it. This result shows that MF is not suitable for the estimation method of the proposed system.

Figures 7 and 9 show that the conventional EKF and proposed EKF can estimate the attitude with high accuracy. However, the difference in estimation accuracy between the proposed EKF and the conventional EKF is not very large. The improvement in the moving and rotating situation is 0.065 degrees, which is lower than the improvement in the stopping and rotating situation of 0.43 degrees. This is because the proposed method can flexibly respond when the motion changes, and the number of times it does so in the moving and rotating situations is small so that the results may be different.

The accuracy of roll and pitch angle estimation using conventional EKF and proposed EKF is higher than that of yaw angle. This is because the accuracy of the information used to estimate the yaw angle is lower than that of the other angles. The roll and pitch angles can be estimated with high accuracy with reference to the direction of gravity. On the other hand, yaw angle can be estimated by multiple GPS, but it is affected by noise more strongly than other sensors because of the close distance (35 cm) between GPS.

3.2. Real Environment Experiment

In this section, we conducted two experiments to verify the performance of the proposed method in a real environment. We carried out two experiments with conditions same as in section 3.1 outdoor. In both experiments, we constructed the drone shown in Fig. 11 for the experiment and estimated the attitude in the outdoor.
We used the sensor BMX055 from Bosch Sensortec for IMU and ZED-F9p from u-blox for GPS. The update frequencies are 30 Hz and 5 Hz, respectively. The drones were connected by bolts rather than electromagnets for ease of handling in the experiment.

3.2.1. Experimental results (stopping and rotating)

In this section, we experimented with a hypothetical situation of repeated stationary and rotational motion in the real world. We used the drone shown in Fig. 11 and a tripod with an angle scale for this experiment. Fig. 12 shows the angle scale mounted on the tripod.
We fixed the drone to a tripod and manually rotated the drone, and rotated the drone 30 degrees every minute using the angle scale as a guide. We performed ten of these rotational movements and compared the accuracy with the estimation results of each method. We extracted scenes (50s $\times$ 10 times) from the video of our experiments where the drone was stationary and compared them in that section. We compared the accuracy at the output of the prediction step by the IMU of the EKF (15,000 times).

Figure 11. The Connected Drone Used in the Outdoor Experiment

Figure 12. Angle Scale Mounted on the Tripod Used During the Experiment

Fig. 13 shows the true value of the yaw angle and the estimation result.

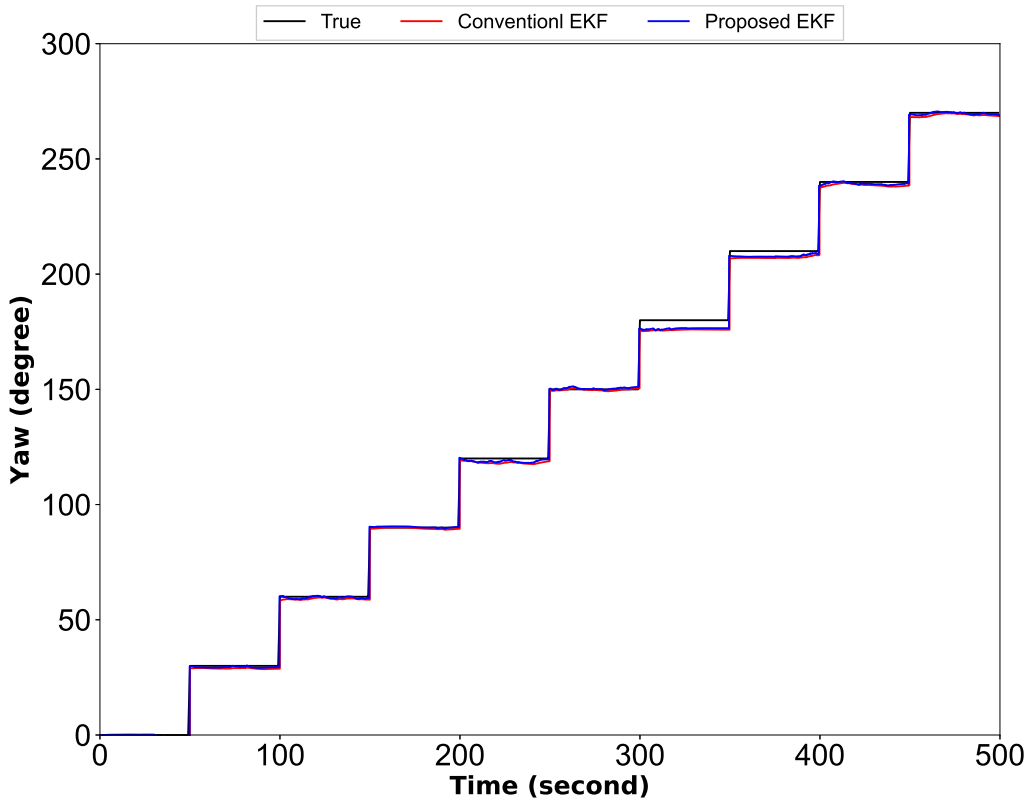

Figure 13. Attitude Estimation Results of Conventional EKF and Proposed EKF (Outdoor Experiment of Stopping and Rotating)

Figure 14 shows the absolute error of Fig. 13 compared to the true value.
MAE and RMSE of each method calculated from these results are shown in Table 3.

Table 3. Comparison results of yaw angle estimation outdoors

	Yaw Angle [°]	
	MAE	RMSE
Conventional EKF[24]	1.49	1.92
Proposed EKF	**1.04**	**1.49**

The proposed method improved MAE by 29.8 % and RMSE by 22.1 % compared with conventional EKF.

3.2.2. Experimental results (moving and rotating)

In this section, we have assessed the accuracy in a continuously moving situation in an outdoor environment. In an open outdoor environment of about 20 m square, as shown in Fig. 15, we moved the drone with it lifted above our heads.

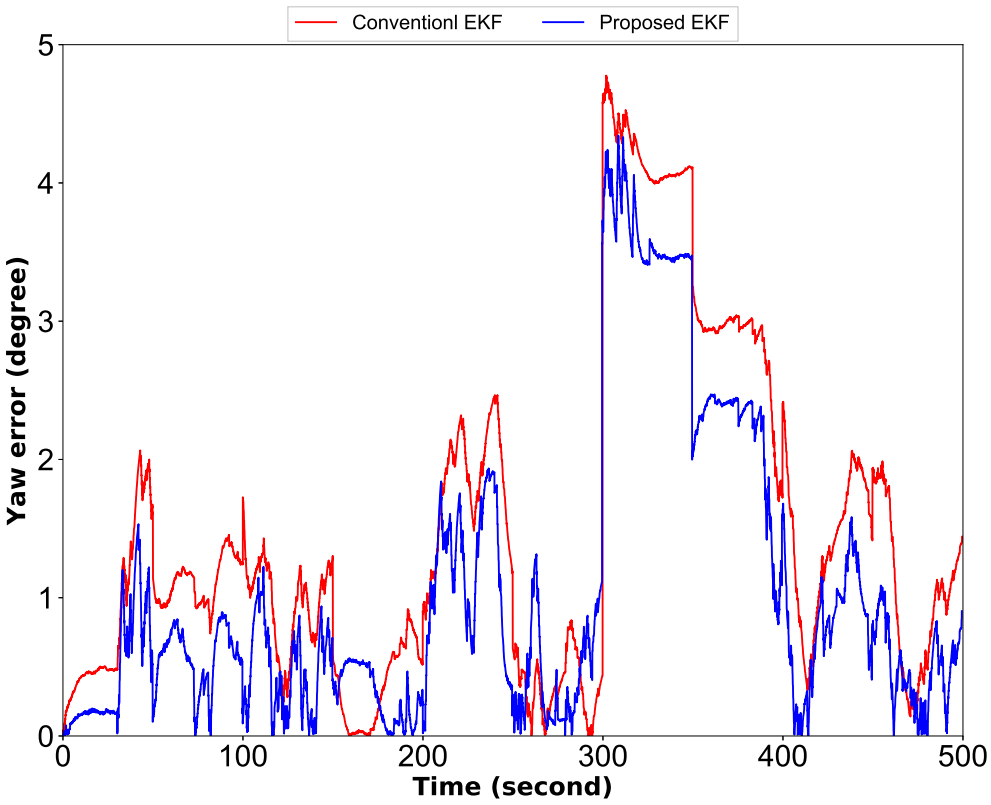

Figure 14. Absolute Error of Attitude Estimation Results of Conventional EKF and Proposed EKF(Outdoor Experiment of Stopping and Rotating)

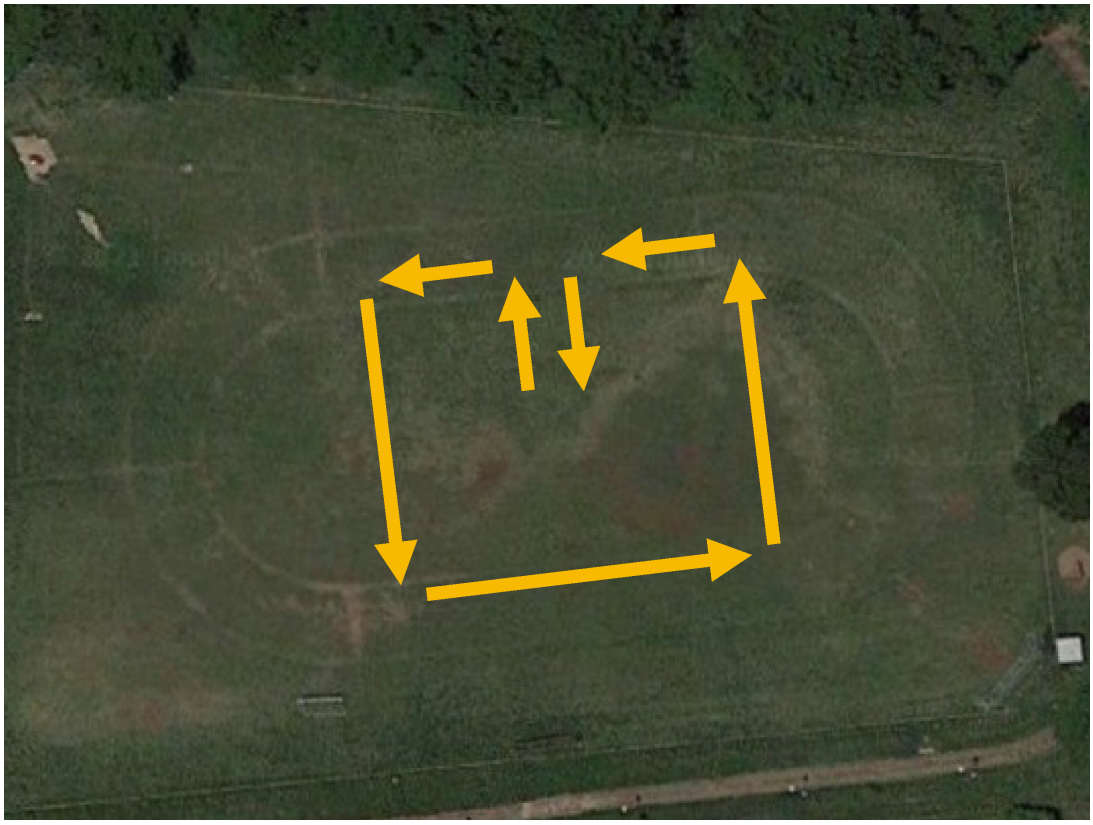

Figure 15. The Route Moved in the Outdoor Experiment

Initially, the drone faces to the right in Fig. 15 and changes direction to the top of Fig. 15. It then repeats, moving forward a certain distance and rotating 90 degrees and returns to the start position. We logged the sensor outputs and input them into two Kalman Filters to verify the stability of the attitude estimation. As it is difficult to measure the true value in this experiment, the stability of the estimation was confirmed.

The estimation using proposed EKF results for the motion in Fig. 15 is shown in Fig. 16.

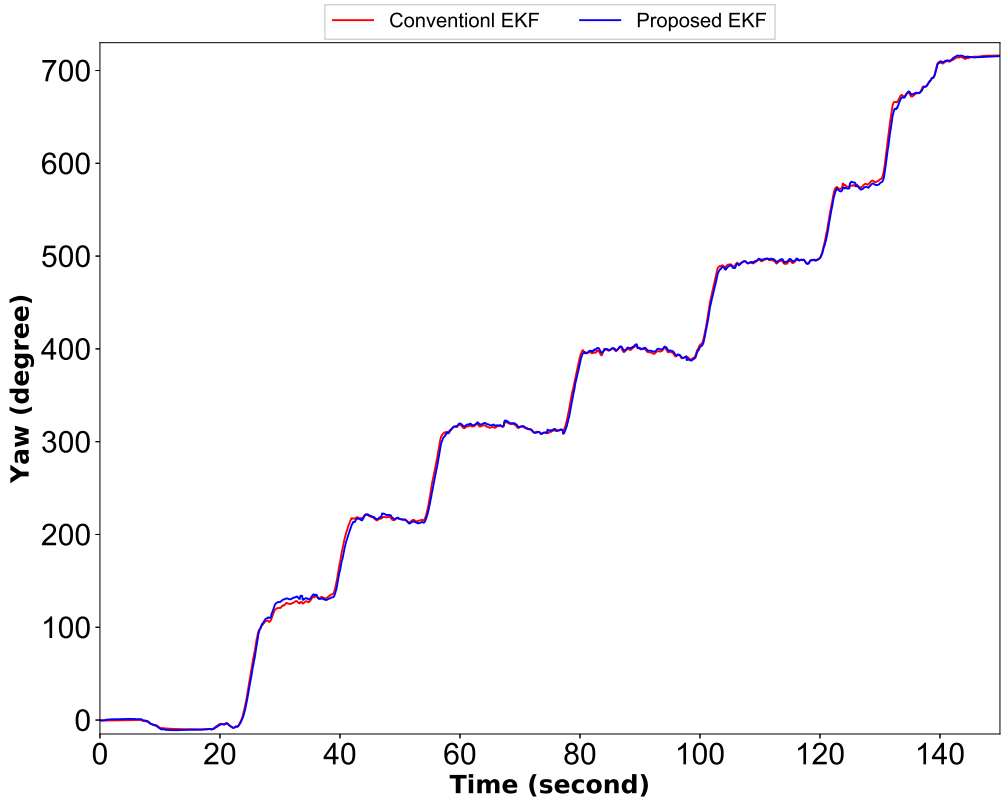

Figure 16. Attitude Estimation Results of Conventional EKF and Proposed EKF(Outdoor Experiment of Moving and Rotating)

3.2.3. Discussion of real environment experiments

Figure 13 showed that the proposed EKF could estimate the yaw angle with high accuracy, but the proposed method only improved accuracy by approximately 0.45 degrees. This could be caused by the lack of benefit of adding the proposed velocity vector because it was a static estimation.

Comparing table 3 with the experimental results of the simulation (table 2), the difference of MAE and RMSE is 0.4 degrees, which means that the simulation experiment can reflect the estimation accuracy of the real environment. Therefore, although we do not measure the true values of the roll and pitch angles in this experiment, the simulation experiment results suggest that the roll and pitch angles are also estimated as accurately as in the simulation.

Figure 16 shows that the proposed EKF can estimate the yaw angle with little

noise, but since the true value is measured by eyeballing the scales, it cannot be measured while moving, and therefore it cannot be compared with the true value in the experiment at section 3.2.2. If we assume that the accuracy is the same as the simulation result (Table 1), the error in Fig. 16 is about 1 degree.

4. Conclusion

In this study, a solution to the problem of attitude estimation in connected drones has been proposed. Specifically, we use multiple GPS instead of the magnetic sensor, which cannot be used due to electromagnets. We have compared the four methods through experiments and shown that the proposed EKF can most accurately estimate. In other words, we have shown that the estimation accuracy can be improved by adding the velocity vector of the drone. We have confirmed estimation accuracy by two types of experiments, one in simulation and the other in the real environment. In the simulation, we have compared the four methods' estimation accuracy in the moving-rotating situation and stopping-rotating situation. As a result, we have found that the proposed method is the best in all situations and angles. In outdoor experiments, we have compared the accuracy of the proposed method with the true value in the stopping situation. As a result, we have found that the proposed method is superior. Although we can not compare with the true value in the moving situation, we have shown that the estimation result is relatively stable. Using proposed method, we can estimate the attitude of a connected drone with a few degrees of error. The accuracy of GPS measurements has a significant impact on estimation accuracy so that the environment in which the proposed method can be used must be open space. However, because the method does not use a magnetic sensor, it is possible to accurately estimate the attitude in an environment where the geomagnetic field is disturbed. In the future, we hope to conduct flight experiments while connecting. Furthermore, estimation experiments in a high-speed environment and the true value comparison experiments with roll angle and pitch angle in a real environment should also be investigated.

Funding

This work was supported by JST CREST under Grant Number JPMJCR1512, Japan.

Disclosure statement

The authors have no conflicts of interest directly relevant to the content of this article.

References

[1] Clarke R. Understanding the drone epidemic. Computer Law & Security Review. 2014; 30(3):230–246.
[2] Nonami K. Dorõn sangyou no ouyou no subete: kaihatsu no kiso kara katsuyou no jissai made [All of the applications in the drone industry: from the basics of development to actual use]. Tokyo, Japan: Ohmsha Ltd.; 2018. Japanese.
[3] Bas V, Huub N, Geert B, et al. Drone Technology: Types, Payloads, Applications, Frequency Spectrum Issues and Future Developments. In: Custers B, editor. The Future of

Drone Use: Opportunities and Threats from Ethical and Legal Perspectives. The Hague, Netherlands: T.M.C. Asser Press; 2016. p. 21–45.
[4] Zhao M, Anzai T, Shi F, et al. Design, modeling, and control of an aerial robot dragon: A dual-rotor-embedded multilink robot with the ability of multi-degree-of-freedom aerial transformation. IEEE Robotics and Automation Letters. 2018;3(2):1176–1183.
[5] Paczan NM, Elzinga MJ, Hsieh R, et al. Collective unmanned aerial vehicle configurations ; 2016. Available from: https://pdfaiw.uspto.gov/.aiw?PageNum=0&docid=20160378108.
[6] Duffy MJ, Bouwer SH, Mattero JJ. Modular vehicle lift system ; 2016. Available from: https://pdfpiw.uspto.gov/.piw?PageNum=0&docid=09457899.
[7] Beaman BS, Kline EV, Rakshit SK. In flight transfer of packages between aerial drones ; 2018. Available from: https://pdfpiw.uspto.gov/.piw?PageNum=0&docid=09561852.
[8] Nonami K, Kendoul F, Suzuki S, et al. Autonomous Flying Robots: Unmanned Aerial Vehicles and Micro Aerial Vehicles. Tokyo, Japan: Springer; 2010.
[9] Ma Z, Chen Z, Huang L. A review: The survey of attitude estimation in autonomous uav navigation. In: Proceedings of the 2019 International Conference on Wireless Communication, Network and Multimedia Engineering (WCNME 2019). Atlantis Press; 2019. p. 50–53.
[10] Adachi S, Maruta I. Karuman firutã no kiso[Fundamentals of kalman filter]. Tokyo, Japan: Tokyo Denki Daigaku Shuppan; 2012. Japanese.
[11] Auger F, Hilairet M, Guerrero JM, et al. Industrial applications of the kalman filter: A review. IEEE Transactions on Industrial Electronics. 2013;60(12):5458–5471.
[12] Ljung L. Asymptotic behavior of the extended kalman filter as a parameter estimator for linear systems. IEEE Transactions on Automatic Control. 1979;24(1):36–50.
[13] Julier SJ, Uhlmann JK. New extension of the kalman filter to nonlinear systems. In: Signal processing, sensor fusion, and target recognition VI; Vol. 3068; International Society for Optics and Photonics; 1997. p. 182–193.
[14] Mohamed A, Schwarz K. Adaptive kalman filtering for ins/gps. Journal of geodesy. 1999; 73(4):193–203.
[15] Chen G, Xie Q, Shieh LS. Fuzzy kalman filtering. Information Sciences. 1998;109(1-4):197–209.
[16] Jing X, Cui J, He H, et al. Attitude estimation for uav using extended kalman filter. In: 2017 29th Chinese Control And Decision Conference (CCDC); IEEE; 2017. p. 3307–3312.
[17] Zheng Y, Dong L, Wang Q. Multi-rotor uav attitude calculation based on extended kalman filter. In: 2018 Chinese Control And Decision Conference (CCDC); IEEE; 2018. p. 478–483.
[18] Sheng G, Gao G. Fusion attitude solving algorithm of four-rotor uav based on improved extended kalman filter. In: 2019 Chinese Automation Congress (CAC); IEEE; 2019. p. 3296–3299.
[19] Tang H, Shen Z. An attitude estimate method for fixed-wing uav s using mems/gps data fusion. In: 2017 First International Conference on Electronics Instrumentation & Information Systems (EIIS); IEEE; 2017. p. 1–5.
[20] Jano D, Arogeti S. Drone's attitude estimation in corridor-like environments. In: 2019 European Conference on Mobile Robots (ECMR); IEEE; 2019. p. 1–6.
[21] Xu P, Wang H, Yang S, et al. Detection of crop heights by uavs based on the adaptive kalman filter. International Journal of Precision Agricultural Aviation. 2021;4(1).
[22] Guo C, Tong X, Liu S, et al. High-precision attitude estimation method of star sensors and gyro based on complementary filter and unscented kalman filter. International Archives of the Photogrammetry, Remote Sensing & Spatial Information Sciences. 2017;42.
[23] Youn W, Rhudy MB, Cho A, et al. Fuzzy adaptive attitude estimation for a fixed-wing uav with a virtual ssa sensor during a gps outage. IEEE Sensors Journal. 2019;20(3):1456–1472.
[24] Aghili F, Salerno A. Driftless 3-d attitude determination and positioning of mobile robots by integration of imu with two rtk gpss. IEEE/ASME Transactions on Mechatronics. 2011;18(1):21–31.

[25] ArduPilot Dev Team. Gps for yaw (aka moving baseline)[internet] ; [cited 2021 May 14]. Available from: https://ardupilot.org/copter/docs/common-gps-for-yaw.html.
[26] Park JY, Kim ST, Lee JK, et al. Method of operating a gis-based autopilot drone to inspect ultrahigh voltage power lines and its field tests. Journal of Field Robotics. 2020; 37(3):345–361.
[27] Fukuda K, Kawai S, Nobuhara H. Attitude estimation by kalman filter based on the integration of imu and multiple gpss and its application to connected drones. In: 2020 59th Annual Conference of the Society of Instrument and Control Engineers of Japan (SICE); IEEE; 2020. p. 1286–1292.
[28] Inoue D, Suzuki T, Amano Y. Real-time estimation of uav position and attitude by using multiple gnss antennas. The Proceedings of JSME annual Conference on Robotics and Mechatronics (Robomec). 2018 12;2018:2P1–L05.
[29] Muranaka N. Shisei kettei [attitude determination]. In: Attitude Control Research Committee, editor. Jinkou eisei no rikigaku to seigyo hando bukku: kiso riron kara ouyou gijutu made [handbook of Dynamics and Control of Satellites: From Basic Theory to Applied Technology]. Tokyo, Japan: Baifukan; 2007. p. 450–454. Japanese.
[30] Wahba G. A least squares estimate of satellite attitude. SIAM review. 1965;7(3):409–409.
[31] Madgwick S. An efficient orientation filter for inertial and inertial/magnetic sensor arrays. Report x-io and University of Bristol (UK). 2010;25:113–118.
[32] Chui CK, Chen G. Kalman Filtering: with Real-Time Applications. Cham, Switzerland: Springer; 2017.
[33] Diebel J. Representing attitude: Euler angles, unit quaternions, and rotation vectors. Matrix. 2006;58(15-16):1–35.
[34] Leffens E, Markley FL, Shuster MD. Kalman filtering for spacecraft attitude estimation. Journal of Guidance, Control, and Dynamics. 1982;5(5):417–429.

Appendices

A. Derivation of Eq. (24)

$\delta\dot{\hat{\boldsymbol{p}}}_i$ from expression Eq. (20) can be expressed as

$$\delta\dot{\hat{\boldsymbol{p}}}_i = \delta\dot{\hat{\boldsymbol{r}}} + (\dot{A} - \dot{\hat{A}})\boldsymbol{e}_i. \tag{30}$$

Here, $\dot{A}$ and $\dot{\hat{A}}$ are

$$\dot{A} = A(\dot{\boldsymbol{q}}), \dot{\hat{A}} = \dot{A}(\hat{\boldsymbol{q}}). \tag{31}$$

Since

$$A(\boldsymbol{q}) = A(\delta\boldsymbol{q} \otimes \hat{\boldsymbol{q}}) = \hat{A}A(\delta\boldsymbol{q}), \tag{32}$$

is derived from Eq. (6) and Eq. (7), the derivative of the rotation matrix A can be calculated as

$$\dot{A} = \dot{\hat{A}}A(\delta\boldsymbol{q}) + \hat{A}A(\dot{\delta}\boldsymbol{q}). \tag{33}$$

$A(\delta q)$ is substituted with Eq. (8) to obtain

$$\dot{A} = \dot{\hat{A}}(I_3 + 2[\delta \boldsymbol{q}_v \times]) + \hat{A}\frac{d}{dt}(I_3 + 2[\delta \boldsymbol{q}_v \times]) \tag{34}$$

$$= \dot{\hat{A}} + 2\dot{\hat{A}}[\delta \boldsymbol{q}_v \times] + 2\hat{A}[\delta \dot{\boldsymbol{q}}_v \times]. \tag{35}$$

Therefore, the second term on the right side of Eq. (30) can be transformed into

$$(\dot{A} - \dot{\hat{A}})\boldsymbol{e}_i \tag{36}$$

$$= (\dot{\hat{A}} + 2\dot{\hat{A}}[\delta \boldsymbol{q}_v \times] + 2\hat{A}[\delta \dot{\boldsymbol{q}}_v \times] - \dot{\hat{A}})\boldsymbol{e}_i \tag{37}$$

$$= -2\dot{\hat{A}}[\boldsymbol{e}_i \times]\delta \boldsymbol{q}_v - 2\hat{A}[\boldsymbol{e}_i \times]\delta \dot{\boldsymbol{q}}_v. \tag{38}$$

Because the last term of Eq. (38), can be calculated from Eq. (11), as

$$-2\hat{A}[\boldsymbol{e}_i \times]\delta \dot{\boldsymbol{q}}_v = -2\hat{A}[\boldsymbol{e}_i \times](-[\hat{\boldsymbol{\omega}} \times]\delta \boldsymbol{q}_v - \frac{1}{2}\delta \boldsymbol{b} - \frac{1}{2}\boldsymbol{w}_g) \tag{39}$$

$$\approx 2\hat{A}[\boldsymbol{e}_i \times][\hat{\boldsymbol{\omega}} \times]\delta \boldsymbol{q}_v + \hat{A}[\boldsymbol{e}_i \times]\delta \boldsymbol{b}. \tag{40}$$

Therefore, Eq. (30) becomes

$$\delta \dot{\hat{\boldsymbol{p}}}_i \approx \begin{bmatrix} 2(\hat{A}[\boldsymbol{e}_i \times][\hat{\boldsymbol{\omega}} \times] - \dot{\hat{A}}[\boldsymbol{e}_i \times]) & 0_3 & I_3 & \hat{A}[\boldsymbol{e}_i \times] \end{bmatrix} \delta \boldsymbol{x}. \tag{41}$$